GEOPHYSICS, VOL. 53, NO. 4 (APRIL 1988); P. 479–491, 11 FIGS.

Rapid computation of multioffset vertical seismic profile synthetic seismograms for layered media

Subhashis Mallick* and L. Neil Frazer*

ABSTRACT

By rearranging the formulas for the responses of buried sources and receivers in the Kennett reflectivity algorithm, we have obtained a new algorithm that is very efficient for computing multioffset VSP synthetic seismograms. The rearrangement of the response formulas is quite general inasmuch as it applies to both isotropic and anisotropic Kennett codes. Our new algorithm and the original single-receiver algorithm can both be made to run much faster on vector computers by taking the layer loop out of the *p*-loop, but leaving it inside the frequency loop. The resulting vector codes can still compute the response of media with frequency-dependent velocities.

INTRODUCTION

Over the past decade, vertical seismic profiling (VSP) has become a widely used tool in seismic exploration. The main reason for its popularity is that it allows one to observe the passage of seismic waves through the earth as they undergo reflections and mode conversions at various interfaces. Even though VSP has gained popularity in the past few years, its basic ideas are relatively old. Dix (1939) used borehole seismometry to determine subweathering velocity from check shots. This application was followed by studies of the propagation of seismic waves from measurements obtained in boreholes (Jolly, 1953; Khalyevich, 1955; Riggs, 1955). Soviet geophysicists especially have contributed greatly to the development of VSP (Gal'perin, 1974). A comprehensive review of the different aspects of VSP is given in Balch and Lee (1984).

With the increased popularity of VSP, there is now a growing need for computing theoretical VSP seismograms as an aid to interpretation. Considerable progress has already been made in this regard: Wyatt (1981), Kelly et al. (1982), Temme and Müller (1982), Ursin and Arnsten (1983), Thybo (1983), Cormier and Mellen (1984), Stephen (1984), and Sullivan (1984) are a few examples. Most of these papers restrict the computation of synthetic VSP seismograms to the case of normal incidence. Dietrich et al. (1984) gave a method which allows offset VSP, but their method encountered difficulties with high frequencies. McMechan (1985) gave a finite-difference algorithm to compute offset VSPs for laterally varying acoustic media. Aminzadeh and Mendel (1985) gave a state-space algorithm and showed how VSPs at nonnormal incidence can be obtained by computing the surface synthetic response first and then continuing that response downward to the given VSP depth points. Even though the method of Aminzadeh and Mendel gives a way to compute offset VSP for a layered elastic medium, it has some practical drawbacks. It does not include surface waves. Also, it assumes the medium to be lossless. The frequency-domain approach discussed here includes surface waves and lossy media.

There are many methods for generating theoretical seismograms for a layered elastic medium; the reflectivity method, originally proposed by Fuchs and Müller (1971) and eventually modified by Kennett (1974, 1975, 1979, 1980), Kind (1976), Stephen (1977), Kennett and Kerry (1979), Kennett and Illingworth (1981), Kennett and Clarke (1983), and Mallick and Frazer (1986) seems most popular. A detailed review of this method may be found in Kennett (1983). Suprajitno and Greenhalgh (1986) used this reflectivity technique to generate offset VSPs for layered media. Their method has the basic advantage of the reflectivity method: a complete response, including all free-surface and internal multiples, is computed at once. Moreover, Suprajitno and Greenhalgh give a way to accommodate deviated holes and offer approximate solutions for some special classes of laterally varying structures such as faults and pinchouts. Their method, however, requires computing the entire reflectivity matrix for each receiver depth. Because the computation of this matrix is the most time-consuming part of the reflectivity method, Suprajitno and Greenhalgh's procedure can only be applied to relatively simple models involving very few layers. The application of synthetic seismograms to interpreting seismic data has shown that exact traveltime and amplitude modeling can only be

Manuscript received by the Editor November 11, 1986; revised manuscript received August 14, 1987.
*Hawaii Institute of Geophysics, University of Hawaii, 2525 Correa Road, Honolulu, HI 96822.

achieved by allowing velocity gradients within geologic formations (e.g., see Braile and Smith, 1975). A model with few layers having constant velocities and densities in each layer may satisfy the traveltimes of the data but to match the amplitudes correctly, one must allow the velocities and densities to vary within each layer as well. Doing so requires subdividing each constant-velocity and constant-density layer into many thin layers; computing a multioffset VSP response for such a multilayered medium places a great premium on speed and efficiency.

Schmidt and Tango (1986) gave a stable form of the global matrix approach (Chin et al., 1984) that is highly efficient for computing the response for multiple receiver and source locations. In this paper, we present a reflectivity approach for computing multioffset VSP which we believe to be at least as efficient as that of Schmidt and Tango, especially in vector computers. The interesting features of our method are as follows:

1) it is based on the reflectivity algorithm, which allows a complete response, including all the free-surface and the interlayer multiples, to be computed at once;
2) intrinsic attenuation may be easily accommodated by making the seismic velocities complex and frequency-dependent;
3) the reflectivity matrix need not be computed repeatedly for each receiver depth;
4) the algorithm can be applied to a general anisotropic model (Fryer and Frazer, 1984); and
5) the algorithm vectorizes efficiently in computers such as a CRAY, resulting in very rapid computation.

THEORY

We consider a multilayered earth, bounded above by a free surface and below by a half-space. The receivers are located at different depths inside a well (arbitrarily spaced) and the sources are located at a single depth but at different offsets (Figure 1). Our object is to find the seismic response from each source at each receiver level. The basic method for the case of a single receiver is thoroughly discussed in Kennett (1983), and the modifications needed for anisotropic media have been given by Fryer and Frazer (1984). We assume a Cartesian coordinate system (x, y, z), where x and y denote the two horizontal (range) coordinates and z denotes the depth coordinate. After we have transformed the horizontal coordinates and time variations out, using a triple Fourier transform of the form

$$\int_{-\infty}^{\infty}\int_{-\infty}^{\infty}\int_{-\infty}^{\infty} f(x, y, z, t)e^{i(\omega t - k_x x - k_y y)}\, dx\, dy\, dt,$$

all the variables become functions of frequency (ω), horizontal wavenumbers (k_x, k_y), and depth z; the subsequent derivations are in this transformed domain. The derivations are valid in general for an anisotropic viscoelastic medium; however, in the case of media exhibiting azimuthal symmetry, e.g., the isotropic or the transversely isotropic case, the variables k_x and k_y appear in the equations of motion in a symmetrical fashion. The first step in our method consists of layer-by-layer iteration and of forming the reflection-transmission coefficient matrix for the entire stack of layers. If for the system shown in Figure 2, $\mathbf{R}_d$ and $\mathbf{T}_d$ are the downward looking reflection and transmission coefficient matrices and $\mathbf{R}_u$ and $\mathbf{T}_u$ are the upward looking reflection and transmission coefficient matrices to depth $z = z_{i-1}^{+}$ and if $\mathbf{r}_d$ and $\mathbf{t}_d$ are downward looking reflection coefficient matrices and $\mathbf{r}_u$ and $\mathbf{t}_u$ are the upward looking reflection and transmission coefficient matrices for the interface at $z = z_i$, then the new reflection and transmission coefficients to depth $z = z_i^{+}$ are given by the iteration relations

$$(\mathbf{T}_u)_{\text{new}} = \mathbf{T}_u(\mathbf{I} - \mathbf{E}_u^{-1}\mathbf{r}_d\mathbf{E}_d\mathbf{R}_u)^{-1}\mathbf{E}_u^{-1}\mathbf{t}_u,$$

$$(\mathbf{R}_d)_{\text{new}} = \mathbf{R}_d + \mathbf{T}_u\mathbf{E}_u^{-1}\mathbf{r}_d\mathbf{E}_d(\mathbf{I} - \mathbf{R}_u\mathbf{E}_u^{-1}\mathbf{r}_d\mathbf{E}_d)^{-1}\mathbf{T}_d,$$

$$(\mathbf{R}_u)_{\text{new}} = \mathbf{r}_u + \mathbf{t}_d\mathbf{E}_d\mathbf{R}_u(\mathbf{I} - \mathbf{E}_u^{-1}\mathbf{r}_d\mathbf{E}_d\mathbf{R}_u)^{-1}\mathbf{E}_u^{-1}\mathbf{t}_u, \quad (1)$$

and

$$(\mathbf{T}_d)_{\text{new}} = \mathbf{t}_d\mathbf{E}_d(\mathbf{I} - \mathbf{R}_u\mathbf{E}_u^{-1}\mathbf{r}_d\mathbf{E}_d)^{-1}\mathbf{T}_d,$$

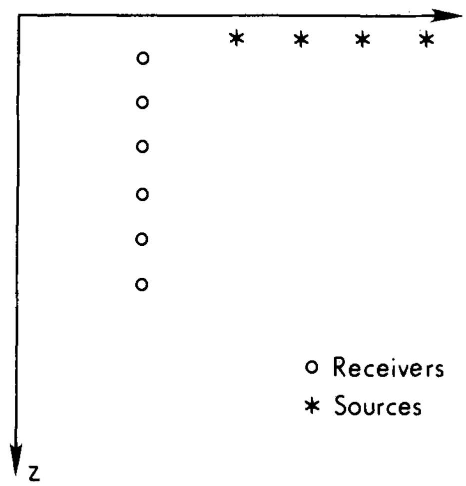

FIG. 1. Geometry for multioffset VSP computations.

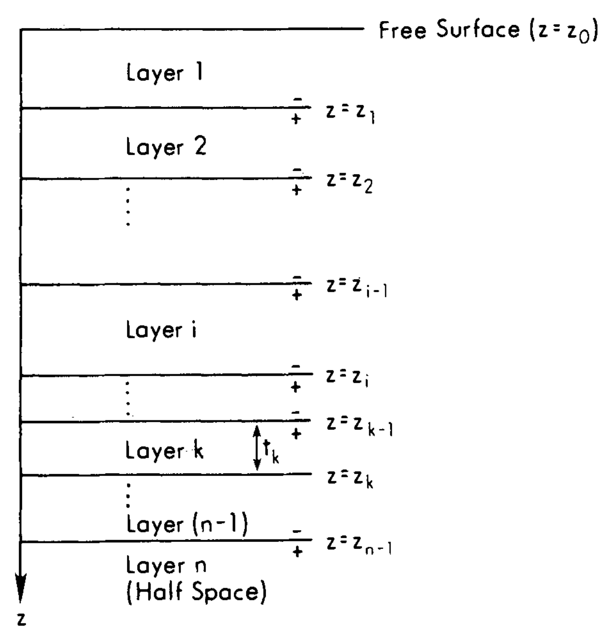

FIG. 2. A stack of layers with different elastic properties. The plus and minus signs denote "just below" or "just above" a particular interface.

where $\mathbf{I}$ is the identity matrix and $\mathbf{E}_u$ and $\mathbf{E}_d$ are the diagonal matrices which downward propagate the upgoing and downgoing waves, respectively, in layer i. In an isotropic or transversely isotropic medium $\mathbf{E}_u^{-1} = \mathbf{E}_d$. In general, matrices in equations (1) are 3×3 and the reflection-transmission coefficient matrices have the form, for example,

$$\mathbf{R}_d = \begin{bmatrix} R_{pp}^d & R_{p1}^d & R_{p2}^d \\ R_{1p}^d & R_{11}^d & R_{12}^d \\ R_{2p}^d & R_{21}^d & R_{22}^d \end{bmatrix}.$$

Here R_{21}^d is the reflection coefficient for a quasi-S_2 wave from a downward incident quasi-S_1 wave; R_{p2}^d is the reflection coefficient for a quasi-P wave from a downward incident quasi-S_2 wave; and so on. For any layer k of thickness $t_k = z_k - z_{k-1}$ (see Figure 2), the matrices $\mathbf{E}_u$ and $\mathbf{E}_d$ are given by

$$\mathbf{E}_u = \begin{bmatrix} e^{i\lambda_1 t_k} & 0 & 0 \\ 0 & e^{i\lambda_2 t_k} & 0 \\ 0 & 0 & e^{i\lambda_3 t_k} \end{bmatrix},$$

and (2)

$$\mathbf{E}_d = \begin{bmatrix} e^{i\lambda_4 t_k} & 0 & 0 \\ 0 & e^{i\lambda_5 t_k} & 0 \\ 0 & 0 & e^{i\lambda_6 t_k} \end{bmatrix},$$

where $\lambda_1, \ldots, \lambda_6$ are the eigenvalues for the 6×6 elastic system matrix $\mathbf{A}$ computed in such a way that the eigenvector matrix $\mathbf{D}$ of $\mathbf{A}$ has the upgoing waves in its first three columns and downgoing waves in its last three columns. Then λ_1, λ_2, and λ_3 are the eigenvalues for the upgoing waves and λ_4, λ_5, and λ_6 are the eigenvalues for the downgoing waves, respectively. A detailed explanation of this development may be found in Fryer and Frazer (1984). In special cases, where the medium exhibits azimuthal symmetry, such as the isotropic or the transversely isotropic case, the whole 6×6 elastic system decouples into a 4×4 P-SV and a 2×2 SH (or quasi-S_2) system. For the P-SV system, the matrix equation (1) becomes 2×2, and for the SH system, it becomes a scalar equation; there are simple and explicit forms for the reflection-transmission coefficients and the transmission matrices for such cases (for example, see Aki and Richards, 1980; Kennett, 1983, chap. 5).

A point source located at $\mathbf{r} = (0, 0, z_s)$ can be represented in terms of a force $\mathbf{h}$ and a symmetric moment tensor $\mathbf{M}$, with the body force equivalent given by (Burridge and Knopoff, 1964)

$$\mathbf{f}(\omega) = \mathbf{h}(\omega)\delta(\mathbf{r} - \mathbf{r}_s) - \mathbf{M}(\omega) \cdot \nabla\delta(\mathbf{r} - \mathbf{r}_s), \tag{3}$$

where δ is the delta function and ∇ denotes the gradient operator. [For an explosive source, $\mathbf{h}(\omega) = 0$ and $\mathbf{M}(\omega)$ is proportional to the identity matrix.] The discontinuity $\mathbf{S}$ in the displacements and vertical components of stress leads to a discontinuity in the amplitudes of the upgoing and downgoing waves given by

$$\mathbf{F} = \begin{bmatrix} -\mathbf{F}_u \\ \mathbf{F}_d \end{bmatrix} = \mathbf{D}^{-1}(z_s)\mathbf{S}(z_s). \tag{4}$$

$\mathbf{D}^{-1}(z_s)$ in equation (4) is the inverse of the eigenvector matrix $\mathbf{D}(z_s)$ of the elastic system matrix $\mathbf{A}(z_s)$. Once $\mathbf{D}$ is found, it is straightforward to find $\mathbf{D}^{-1}$ (Fryer and Frazer, 1984). For the general case $\mathbf{D}$ must be found numerically; however, for the isotropic and for the transversely isotropic case, the 4×4 $\mathbf{D}$ matrix for P-SV and 2×2 $\mathbf{D}$ matrix for SH can be explicitly found [see Kennett, 1983, equation (3.37), for example, for the isotropic case]. The vector $\mathbf{S}(z_s)$ in equation (4) is obtained from equation (3), by Fourier transformation over x and y, in the form

$$\mathbf{S}(z_s) = \begin{bmatrix} 0 \\ 0 \\ 0 \\ ih_x + k_x M_{xx} + k_y M_{xy} \\ ih_y + k_y M_{xy} + k_y M_{yy} \\ ih_z + k_x M_{zx} + k_y M_{zy} \end{bmatrix} - \mathbf{A}(z_s) \begin{bmatrix} 0 \\ 0 \\ 0 \\ M_{xz} \\ M_{yz} \\ M_{zz} \end{bmatrix}. \tag{5}$$

Finally, in order to get the motion $\mathbf{u}(z_r)$ at the arbitrary receiver location $z = z_r$, the matrix $\mathbf{D}(z_r)$ is first written in terms of submatrices as

$$\mathbf{D} = \left[\begin{array}{c|c} \mathbf{M}_u^r & \mathbf{M}_d^r \\ \hline \mathbf{N}_u^r & \mathbf{N}_d^r \end{array}\right]. \tag{6}$$

Then, for the receiver above the source (Figure 3a), the motion is

$$\mathbf{u}(z_r) = (\mathbf{M}_u^r + \mathbf{M}_d^r \mathbf{R}_u^{rf})(\mathbf{I} - \mathbf{R}_d^{rs}\mathbf{R}_u^{rf})^{-1} \times \mathbf{T}_u^{sr}(\mathbf{I} - \mathbf{R}_d^{sn}\mathbf{R}_u^{sf})^{-1}(\mathbf{R}_d^{sn}\mathbf{F}_d + \mathbf{F}_u); \tag{7a}$$

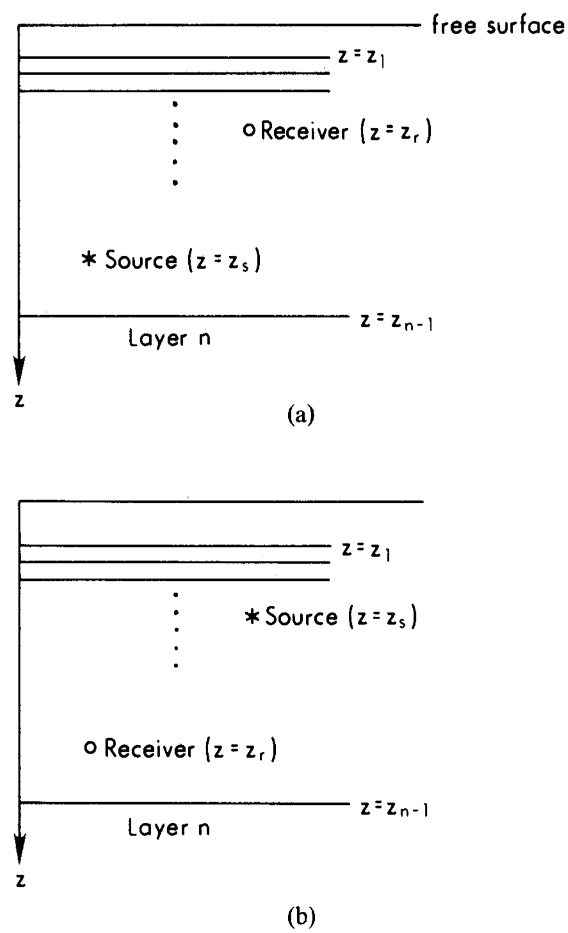

FIG. 3. Layered earth problem when a receiver is (a) above the source and (b) below the source.

```
Frequency loop
    Compute Final p (FP), # of p (NP), delta p (DP)
      ⋮
    Layer Loop
        p loop
                Iteration equations to compute
                R_d, T_d, R_u, T_u
        end p loop
        If source layer then
            p loop
                T_u^sf = T_u; R_u^fs = R_u
                R_d = 0 ; T_d = 0 ; R_u = 0 ; T_u = 0
            end p loop
        else if receiver layer then
            p loop
                R_d^rf = R_d ; T_d^fr = T_d ; R_u^rf = R_u ; T_u^rf = T_u
            end p loop
        end if
    end layer loop
    Receiver loop
        If receiver above source then
            p loop
                compute using equation (12)
            end p loop
        else
            p loop
                compute using equation (14)
            end p loop
        end if
      x loop
        p loop
            integrate over p to transform p to x
        end p loop
      end x loop
    end receiver loop
    write out response for this frequency
end frequency loop
```

FIG. 4. The basic flow chart for computing synthetic VSPs for different offsets.

and for the receiver below the source (Figure 3b),

$$\mathbf{u}(z_r) = (\mathbf{M}_u^r \mathbf{R}_d^{rn} + \mathbf{M}_d^r)(\mathbf{I} - \mathbf{R}_u^{rs}\mathbf{R}_d^{rn})^{-1} \times \mathbf{T}_d^{sr}(\mathbf{I} - \mathbf{R}_u^{sf}\mathbf{R}_d^{sn})^{-1}(\mathbf{F}_d + \mathbf{R}_u^{sf}\mathbf{F}_u). \tag{7b}$$

The notation used in equations (7a) and (7b) is explicit; for example, $\mathbf{R}_d^{rn}$ denotes the downward looking reflection coefficient matrix between z_n (bottom of the stack) and z_r (receiver depth). Similarly, $\mathbf{R}_u^{sf}$ denotes the upward looking reflection coefficient matrix for the stack between z_s and the free surface, and so on.

Finally, by applying the triple Fourier transform

$$\frac{1}{(2\pi)^3}\int_{-\infty}^{\infty}\int_{-\infty}^{\infty}\int_{-\infty}^{\infty}\mathbf{u}(k_x, k_y, z, \omega)e^{i(k_x x + k_y y - \omega t)}\,dk_x\,dk_y\,d\omega, \tag{8}$$

we get the synthetic seismogram for a point source. In the case of an isotropic or a transversely isotropic system, the point-source synthetics are obtained through the Fourier-Hankel transform over the frequency and wavenumber (see Kennett, 1983, chap. 7, for details).

Equations (7a) and (7b) also give a very convenient way to compute the upgoing and downgoing wave responses separately. To see why this is so, recall that the matrices $\mathbf{M}_u^r$ and $\mathbf{M}_d^r$ are the submatrices of the eigenvector matrix $\mathbf{D}$ at each receiver location. The columns of $\mathbf{M}_u^r$ give the upgoing wave displacement and the columns of $\mathbf{M}_d^r$ give the downgoing wave displacement. Thus, if we set $\mathbf{M}_u^r = \mathbf{0}$, equations (7a) and (7b) give the downgoing wave only. Similarly, setting $\mathbf{M}_d^r = \mathbf{0}$ in equations (7a) and (7b) gives the upgoing wave only. Each column of the matrices $\mathbf{M}_u^r$ and $\mathbf{M}_d^r$ represents a different wave type. For an isotropic *P-SV* system for example, the first column gives the *P*-wave motion, and the second column gives the *SV*-wave motion. Thus, setting the second column of $\mathbf{M}_u^r$ to zero and also setting $\mathbf{M}_d^r$ to zero make equations (7a) and (7b) give the upgoing *P*-wave motion only. Upgoing *S*, downgoing *P*, and downgoing *S*-wave motions are obtained in a similar manner. Once the entire reflectivity matrix is computed, these separate motions can be obtained at very little additional expense.

In order to extend this procedure to the VSP case, we examine equations (7a) and (7b) to see how they are used to compute the response in the case of a single receiver depth. The computation is performed through layer-by-layer iteration using equations (1), so that at the ith stage of iteration $\mathbf{R}_u$, $\mathbf{T}_u$, $\mathbf{R}_d$, and $\mathbf{T}_d$ denote the upward and downward looking reflection-transmission coefficient matrices down to layer i. From the top of the stack until the source or the receiver layer is encountered, we compute $\mathbf{R}_u$ only. At the source or the receiver layer (whichever is shallowest), we store this value of $\mathbf{R}_u$, reset $\mathbf{R}_u$ to zero, and start computing $\mathbf{R}_u$, $\mathbf{R}_d$, $\mathbf{T}_u$, and $\mathbf{T}_d$. When the source or receiver layer (whichever is deepest) is encountered, we store the values of $\mathbf{R}_u$, $\mathbf{R}_d$, $\mathbf{T}_u$, and $\mathbf{T}_d$, reset $\mathbf{R}_u$, $\mathbf{R}_d$ to zero and $\mathbf{T}_u$, $\mathbf{T}_d$ to unity, and keep computing the reflection transmission coefficient matrices using equations (1). Finally when the bottom of the stack is encountered, we store $\mathbf{R}_d$. We store the $\mathbf{M}_u^r$ and $\mathbf{M}_d^r$ matrices at the receiver depth. Thus, when the layer iteration is complete, we have for the receiver above the source

(1) $\mathbf{R}_u^{rf}$, $\mathbf{M}_u^r$, $\mathbf{M}_d^r$,
(2) $\mathbf{R}_u^{sr}$, $\mathbf{T}_u^{sr}$, $\mathbf{R}_d^{rs}$, $\mathbf{T}_d^{rs}$, and
(3) $\mathbf{R}_s^{sn}$.

We have all the matrices to compute $\mathbf{u}(z_r)$, using equation (7a), except $\mathbf{R}_u^{sf}$. To find $\mathbf{R}_u^{sf}$, we make use of Kennett's iteration equations [see Kennett, 1983, equation (6.4)] to write

$$\mathbf{R}_u^{sf} = \mathbf{R}_u^{sr} + \mathbf{T}_d^{sr}\mathbf{R}_u^{rf}(\mathbf{I} - \mathbf{R}_d^{rs}\mathbf{R}_u^{rf})^{-1}\mathbf{T}_u^{rs}. \tag{9}$$

Thus, we can now compute $\mathbf{u}(z_r)$ for the case when the receiver is located above the source.

Similarly, for the receiver below the source, when we come out of the layer loop, we have

(1) $\mathbf{R}_u^{sf}$,
(2) $\mathbf{R}_u^{rs}$, $\mathbf{T}_u^{rs}$, $\mathbf{R}_d^{sr}$, $\mathbf{T}_d^{sr}$, $\mathbf{M}_u^r$, $\mathbf{M}_d^r$, and
(3) $\mathbf{R}_d^{rn}$.

We see that we need $\mathbf{R}_d^{sn}$ to compute $\mathbf{u}(z_r)$ using equation (7b). For this we again follow Kennett [1983, equation (6.3)] to write

$$\mathbf{R}_d^{sn} = \mathbf{R}_d^{sr} + \mathbf{T}_u^{rs}\mathbf{R}_d^{rn}(\mathbf{I} - \mathbf{R}_u^{rs}\mathbf{R}_d^{rn})^{-1}\mathbf{T}_d^{sr}. \tag{10}$$

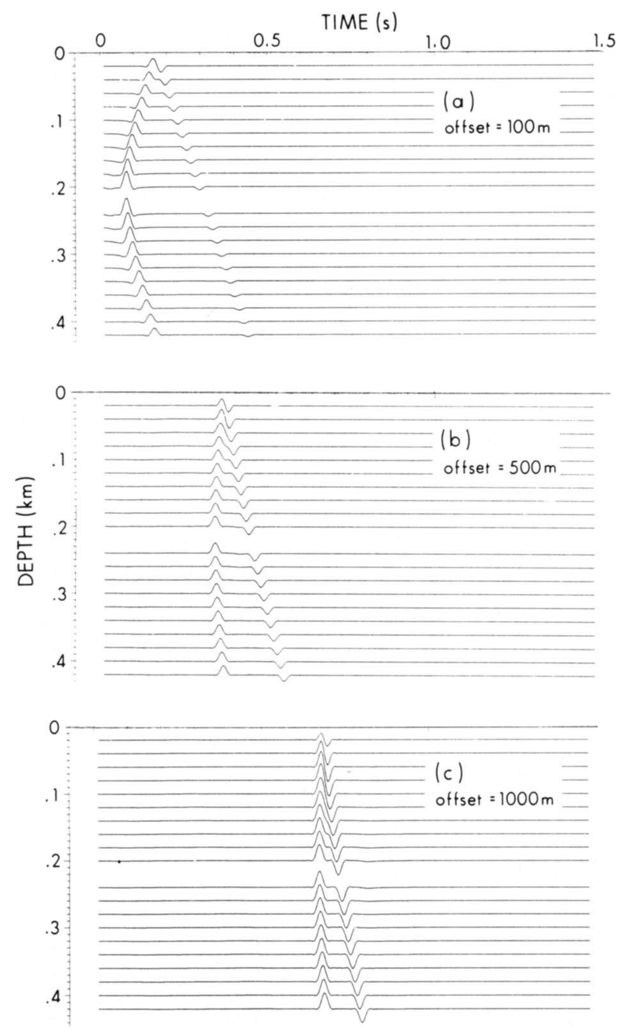

FIG. 5. Synthetic VSP seismograms for the pressure response obtained at (a) 100, (b) 500, and (c) 1000 m offsets for an acoustic half-space with velocity = 1510 m/s and Q = 5000. The source is located 220 m below the free surface and receivers are at 20 m intervals above and below the source.

Thus we get the motion $\mathbf{u}(z_r)$, when the receiver is located below the source.

For the VSP case, when receivers are located at many depths (some above and some below the source), the above procedure is inconvenient because one cannot get all the matrices present in equations (7a) and (7b) in a single pass through the layer loop. Therefore, we need to modify equations (7a) and (7b) into a form convenient for VSP computation. As shown in Figure 3a, for the receiver above the source we may write [Kennett, 1983, equation (6.4)]

$$\mathbf{T}_u^{sf} = \mathbf{T}_u^{rf}(\mathbf{I} - \mathbf{R}_d^{rs}\mathbf{R}_u^{rf})^{-1}\mathbf{T}_u^{sr}. \tag{11}$$

If this expression is solved for $\mathbf{T}_u^{sr}$ and the result substituted into equation (7a), we find

$$\mathbf{u}(z_r) = (\mathbf{M}_u^r + \mathbf{M}_d^r\mathbf{R}_u^{rf})(\mathbf{T}_u^{rf})^{-1} \times \mathbf{T}_u^{sf}(\mathbf{I} - \mathbf{R}_d^{sn}\mathbf{R}_u^{sf})^{-1}(\mathbf{R}_d^{sn}\mathbf{F}_d + \mathbf{F}_u). \tag{12}$$

Similarly, for the receiver below the source (Figure 3b), we have from Kennett [1983, equation (6.3)]

$$\mathbf{R}_d^{sn} = \mathbf{R}_d^{sr} + \mathbf{T}_u^{rs}\mathbf{R}_d^{rn}(\mathbf{I} - \mathbf{R}_u^{rs}\mathbf{R}_d^{rn})^{-1}\mathbf{T}_d^{sr}. \tag{13}$$

Solving this relation for $\mathbf{R}_d^{rn}$ and substituting into equation (7b) yields

$$\begin{aligned}\mathbf{u}(z_r) = &\left[\mathbf{M}_u^r(\mathbf{T}_d^{sr}\mathbf{R}^{-1}\mathbf{T}_u^{rs} + \mathbf{R}_u^{rs})^{-1} + \mathbf{M}_d^r\right] \\ &\times \left[\mathbf{I} - \mathbf{R}_u^{rs}(\mathbf{T}_d^{sr}\mathbf{R}^{-1}\mathbf{T}_u^{rs} + \mathbf{R}_u^{rs})^{-1}\right]^{-1} \\ &\times \mathbf{T}_d^{sr}(\mathbf{I} - \mathbf{R}_u^{sf}\mathbf{R}_d^{sn})^{-1}(\mathbf{F}_d + \mathbf{R}_u^{sf}\mathbf{F}_u),\end{aligned} \tag{14}$$

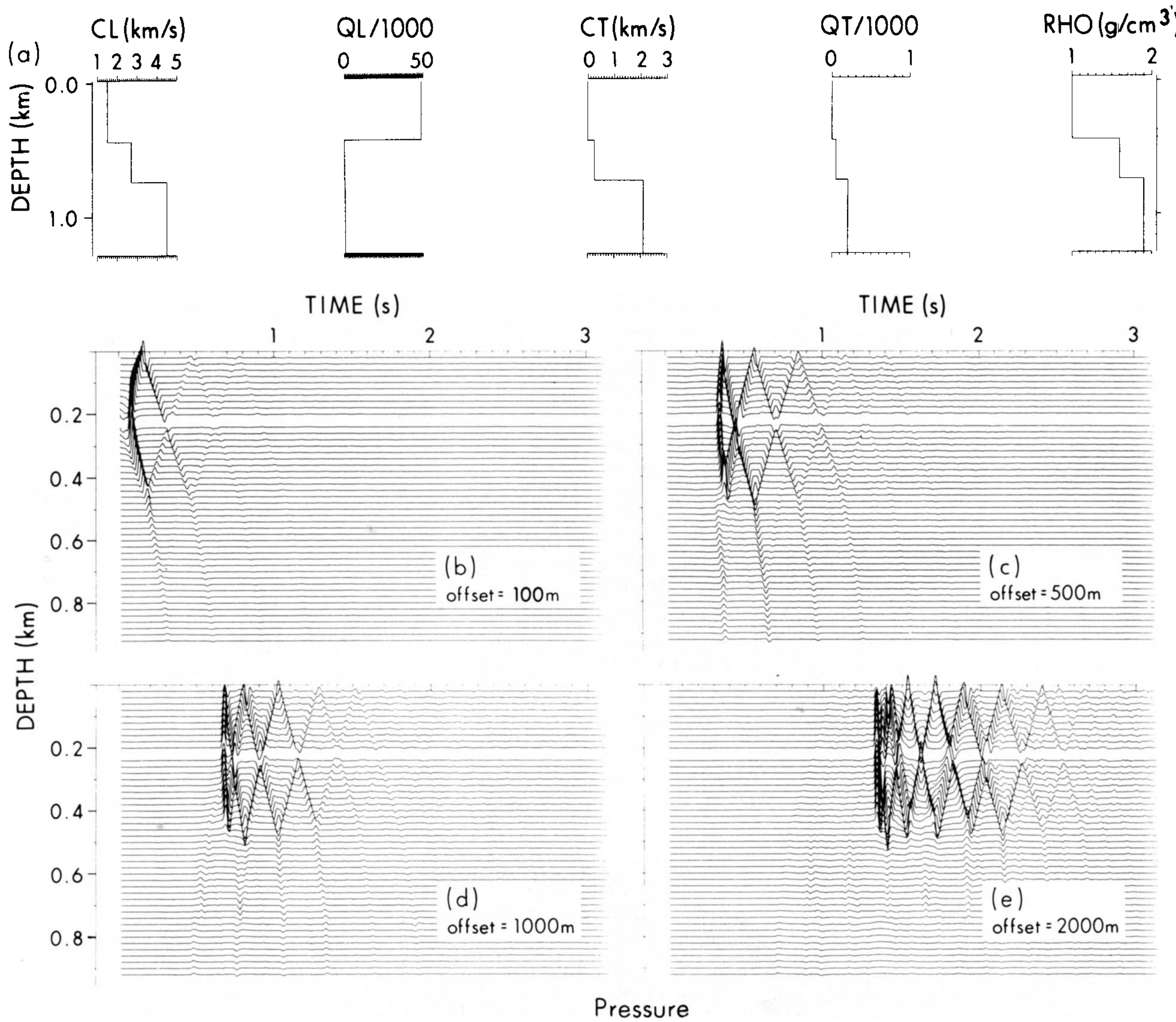

Fig. 6. (a) Longitudinal wave velocity (CL), longitudinal Q (QL), shear-wave velocity (CT), shear Q (QT), and density (RHO) of the model for which the synthetics (b)–(e) were computed. The source was located at a depth of 220 m within the first layer, and 45 receivers were placed at 20 m intervals above and below the source. (b) Computed synthetic VSP seismogram for pressure response using the model shown in (a) at a 100 m offset. (c), (d), and (e) are the same as (b) but at 500, 1000, and 2000 m offsets, respectively.

where

$$\underset{\sim}{R} = \underset{\sim}{R}_d^{sn} - \underset{\sim}{R}_d^{sr}.$$

Equations (12) and (14) give a convenient form for computing the response in a separate receiver loop after passage through the layer loop. To see why this is so, we refer to Figure 4. In the layer loop, as $\underset{\sim}{R}_u$, $\underset{\sim}{T}_u$, $\underset{\sim}{R}_d$, and $\underset{\sim}{T}_d$ are formed using equations (1), when the source layer is encountered, we store the matrices up to this point and reset the reflection matrices to zero and the transmission matrices to unity. However, when a receiver layer is encountered, we simply store the matrices up to this point but do not reset them. Also, we store the $\underset{\sim}{M}_u^r$ and $\underset{\sim}{M}_d^r$ matrices for each receiver location. Thus, after exiting the layer loop, we have

(1) $\underset{\sim}{R}_u^{rf}$, $\underset{\sim}{T}_u^{rf}$, for the receivers above the source,
(2) $\underset{\sim}{R}_u^{sf}$, $\underset{\sim}{T}_u^{sf}$,
(3) $\underset{\sim}{R}_u^{rs}$, $\underset{\sim}{T}_u^{rs}$, $\underset{\sim}{T}_d^{sr}$ for the receivers below the source,
(4) $\underset{\sim}{R}_d^{sn}$, and
(5) $\underset{\sim}{M}_u^r$, $\underset{\sim}{M}_d^r$ for each receiver depth.

Now, looking at equations (12) and (14), it is evident that we have everything necessary to compute the displacement response for each receiver location in a separate receiver loop as shown in Figure 4.

Equations (12) and (14) thus give a complete VSP response for the receivers above and below the source, respectively. However, they are not the only possible arrangement for a VSP computation by the reflectivity method. The reflectivity formulation is very flexible and many different but equivalent forms exist. We prefer equations (12) and (14) because they result in a computer code that has proven stable under a variety of conditions for many different models. To see why this is so, note that equation (12) requires computation of the inverse of the matrix $\underset{\sim}{T}_u^{rf}$. When this matrix tends to zero, computing its inverse will cause numerical instability. However, at the large values of slowness for which $\underset{\sim}{T}_u^{rf}$ tends to zero, the matrix $\underset{\sim}{T}_u^{sf}$ tends to zero faster than $\underset{\sim}{T}_u^{rf}$. Thus, for very large slowness the product $(\underset{\sim}{T}_u^{rf})^{-1}\underset{\sim}{T}_u^{sf}$ is always small and the contribution to the integral in equation (8) is also very small. We never need to compute our synthetics to such high values of slowness. Therefore, in all practical cases of seismogram synthesis, we never encounter numerical instability in using equation (12).

Similarly, equation (14) requires computation of the inverse of the matrix $\underset{\sim}{R} = \underset{\sim}{R}_d^{sn} - \underset{\sim}{R}_d^{sr}$. When $\underset{\sim}{R}_d^{sn}$ and $\underset{\sim}{R}_d^{sr}$ are very close to each other, computing $\underset{\sim}{R}^{-1}$ will cause numerical instability. However, when $\underset{\sim}{R}_d^{sr} \to \underset{\sim}{R}_d^{sn}$, then $\underset{\sim}{R}_d^{rn} = (\underset{\sim}{T}_d^{sr}\underset{\sim}{R}^{-1}\underset{\sim}{T}_u^{rs} + \underset{\sim}{R}_u^{rs})^{-1} \to \underset{\sim}{0}$. Therefore in our computer code, whenever $\underset{\sim}{R}$ is small, instead of computing $\underset{\sim}{R}^{-1}$, we replace the entire matrix $(\underset{\sim}{T}_d^{sr}\underset{\sim}{R}^{-1}\underset{\sim}{T}_u^{rs} + \underset{\sim}{R}_u^{rs})^{-1}$ in equation (14) by zero and thus avoid the instability.

In our computer code we have put the layer loop outside the ray parameter (p) loop (see Figure 4). The original p loop becomes a long chain of p loops, each of which vectorizes. The receiver loop, which follows the p loop and performs the transformation back to space coordinates, also contains p loops which vectorize. We found that this unconventional architecture increased the speed of our code by a factor of seven on a CRAY X-MP.

EXAMPLES

In this section we present two sets of examples. The first set consists of relatively simple models involving only a few layers. These examples are meant to show the correctness of our computation. The second set of examples is for models with complicated velocity structures. These examples are meant to show the efficiency of our method in computing multioffset synthetic VSPs for various complicated geologic models. In all the examples shown the source was an explosion. The source time function was an impulse response, band-limited by means of a frequency-domain Hanning window up to a maximum frequency of 51.2 Hz. Time series wraparound was avoided by making use of complex frequencies (e.g., Mallick and Frazer, 1987). The Q models shown in all the examples are for a reference frequency of 1 Hz. Complex P and S velocities were recomputed for each frequency using the modified Strick power law formula [Mallick and Frazer, 1987, equation (28)] with $\sigma = 0.1$ and $\varepsilon = 0.001$; however, the absorption band model of Liu et al. (1976) could equally well have been used.

The first set of computations consists of three examples. The first example is an acoustic half-space, bounded above by a free surface. We used a water velocity of 1510 m/s, a Q of 5000, and a density of 1 g/cm^3. The source is located 220 m below the free surface and receivers are located at 20 m intervals above and below the source. The synthetic VSP responses for pressure at different receiver levels and for source offsets of 100, 500, and 1000 m are shown in Figure 5. The second example is an acoustic-elastic example. The model is shown in Figure 6a and the VSP synthetics for the pressure responses for different source offsets are presented in Figures 6b–6e. The third and last examples in this set show a four-layer all-elastic model with a low-velocity zone. This model is presented in Figure 7a, and the VSP synthetics for the horizontal and vertical displacement responses at different source offsets are shown in Figure 7b–7g. Figure 8 shows downgoing P-waves, upgoing P-waves, downgoing S-waves, and upgoing S-waves, respectively, at 1500 km offset for the same model presented in Figure 7a. The separate waves for the 500 m and 1000 m offsets are omitted here to save space. As noted earlier, these separate synthetics are obtained with very little extra expense.

The second set of computations consists of three examples. The first example is a simulation of a land VSP using a complex 142-layer model with low-velocity zones and velocity gradients. The source was placed 50 m below the free surface and 48 receivers were placed below the source at 50 m intervals. The model is shown in Figure 9a, and the computed VSP synthetics at different source offsets are shown in Figures 9b–9g. The last two examples are for the oceanic model shown in Figure 10a. It consists of a 3500 m thick ocean that underlies a 200 m ice cap and overlies a typical section of oceanic crust and upper mantle. One hundred seventy-two layers were needed to get the smooth gradient zones in this model. In the first example with this model, a pressure source was placed 25 m below the bottom of the ice, and 48 receivers were placed in the sediment and the basement at 25 m intervals. The computed synthetics are presented in Figures 10b–10g. For the second example, the ice cap was replaced by water, and the VSP synthetics for the same source and receiver geometry are presented in Figures 11a–11f.

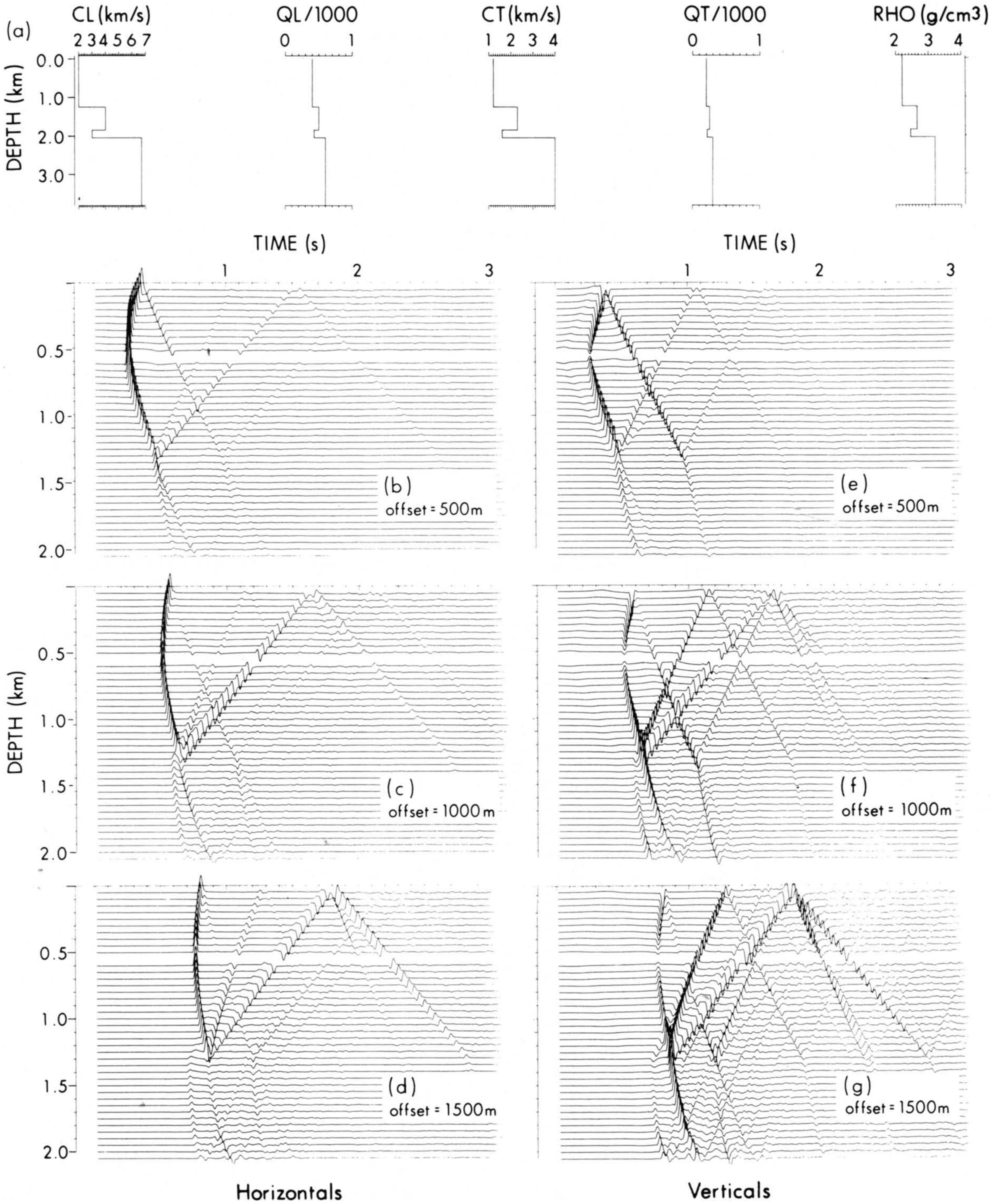

FIG. 7. (a) Longitudinal wave velocity (CL), longitudinal Q (QL), shear-wave velocity (CT), shear Q (QT), and density (RHO) of the model for which the synthetics shown in (b)–(g) were computed. The source was placed at a depth of 550 m in the first layer, and 45 pressure receivers were placed above and below the source at 50 m intervals. (b)–(d) are computed VSP seismograms for horizontal displacement using the model shown in (a) at 500, 1000, and 1500 m offsets, respectively. (e)–(g) are the same as (b)–(d), but with vertical displacement.

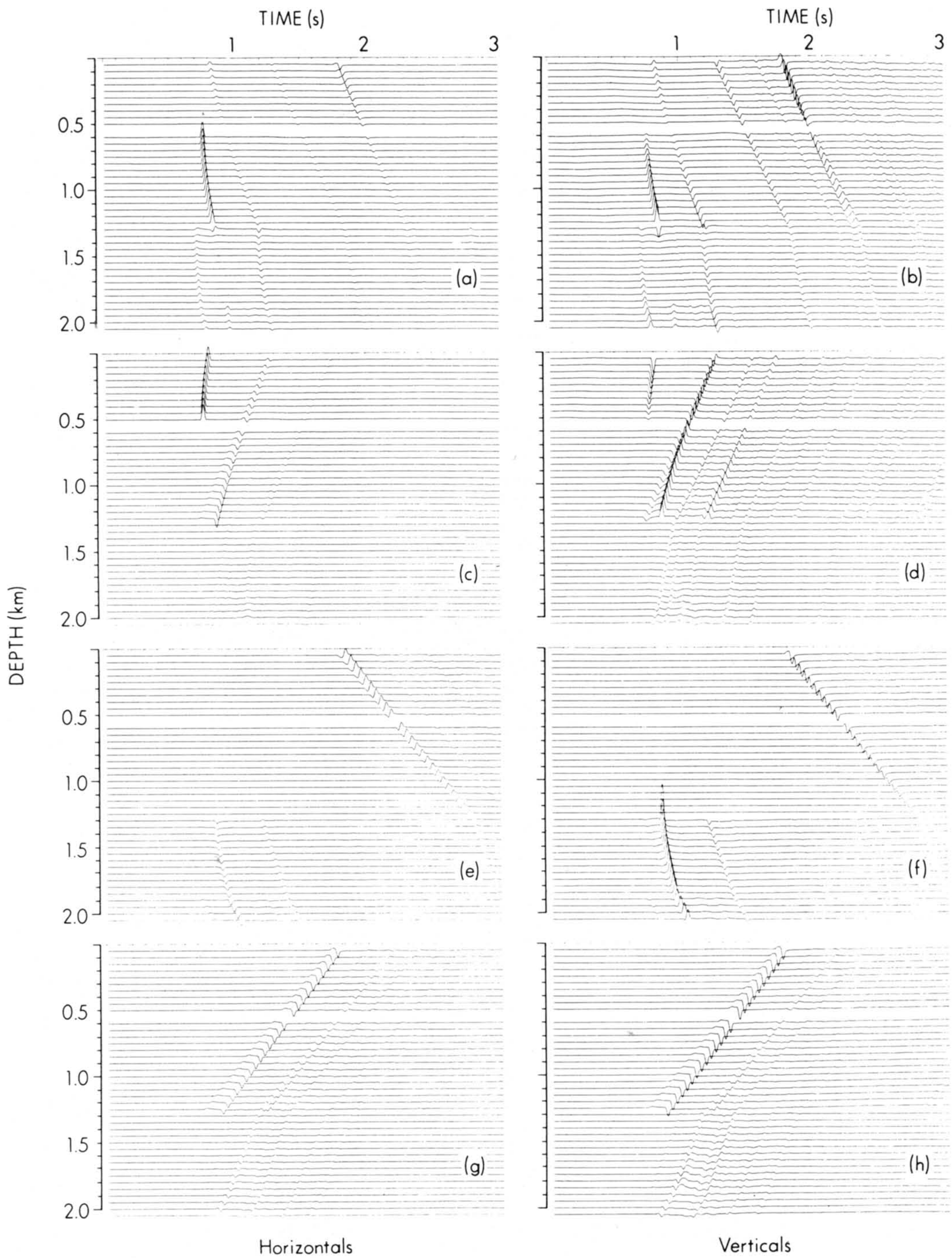

FIG. 8. Here the motions for the 1500 m offset with the model of Figure 7a are shown decomposed into different wave types: (a) and (b), downgoing P; (c) and (d), upgoing P; (e) and (f) downgoing S; (g) and (h), upgoing S. Plots (a), (c), (e), and (g) sum to give Figure 7d. Plots (b) (d), (f), and (h) sum to give Figure 7g.

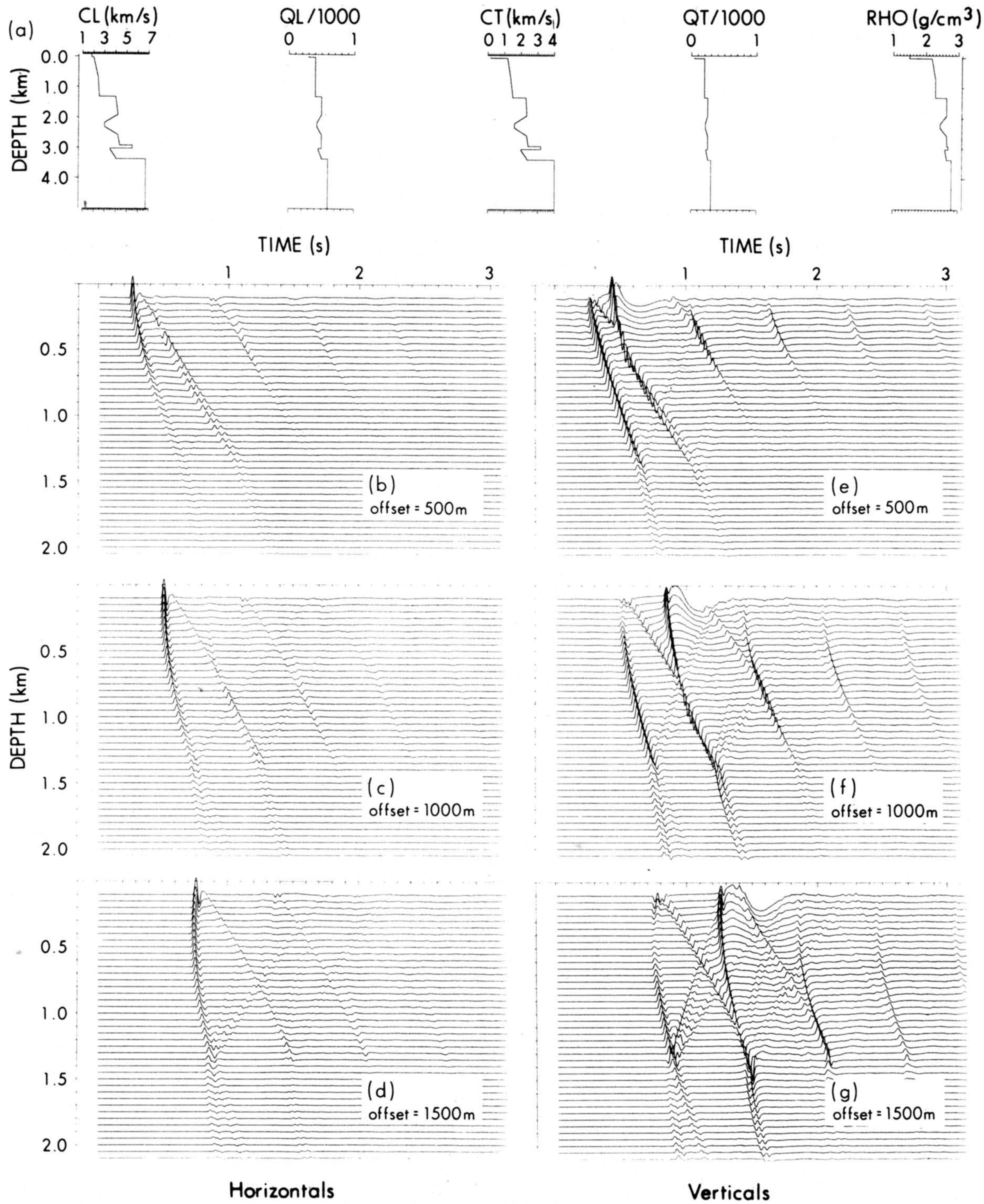

FIG. 9. (a) Longitudinal wave velocity (CL), longitudinal Q (QL), shear-wave velocity (CT), shear Q (QT), and density (RHO) model with which the synthetics shown in (b)–(g) were computed. (b)–(d): synthetic VSP seismograms for horizontal displacement at 500, 1000, and 1500 m offsets, respectively, computed with the model shown in Figure 8a. (e)–(g) are the same as (b)–(d), but with vertical displacement.

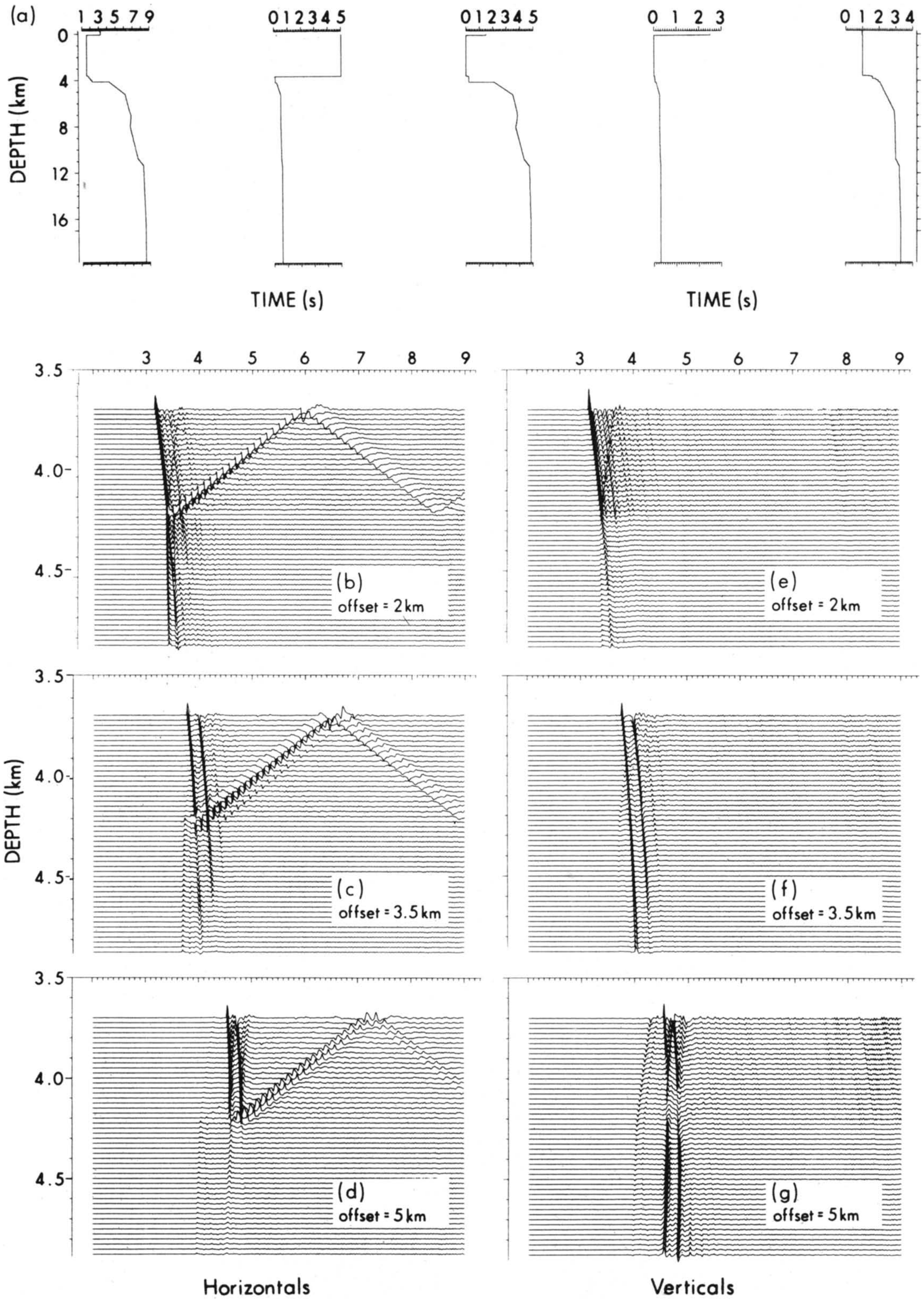

FIG. 10. (a) Longitudinal wave velocity (CL) longitudinal Q (QL), shear-wave velocity (CT), shear Q (QT), and density (RHO) model, with which the synthetics in (b)–(g) were computed. (b)–(d): synthetic VSP seismograms for horizontal displacement at 2, 3.5, and 5, km offsets, respectively, computed with the model shown in Figure 9a. (e)–(g) are the same as (b)–(d), but with vertical displacement.

DISCUSSION

We have outlined a method by which multioffset VSP seismograms can be generated for layered media with frequency-dependent complex velocities. This method is based on the reflectivity approach and is vectorizable on the computers such as a CRAY. Examples for a variety of simple and complex models show that this method is extremely fast and efficient. Computation of all the synthetics in Figures 7 and 8 took less than 3 minutes of CPU time, and computation of all the synthetics in Figure 10 took 30 minutes of CPU time on a CRAY X-MP. In practice, it is therefore possible to compute the offset VSP with this method for realistic geologic models. Examples given for the oceanic model (see Figures 10 and 11) suggest that even though VSP is not a very common technique in the exploration of the deep ocean basins, its application in conjunction with standard refraction experiments could become useful. For example, the VSP synthetics clearly show a strong *P*-to-*P* reflection and relatively weak *P*-to-*S* reflection at the sediment-basement interface on the response from the vertical displacement. On the horizontal motion detectors, however, the effect is opposite (see Figure 11 where these events are marked as *PP* and *PS*, respectively). Such observations can be used to restrict the elastic properties at these zones. Since the reflections are not as clear on the refraction data as they are on the VSP, a combination of the two techniques could be used to expand our knowledge of the structure of the upper crust in the oceans.

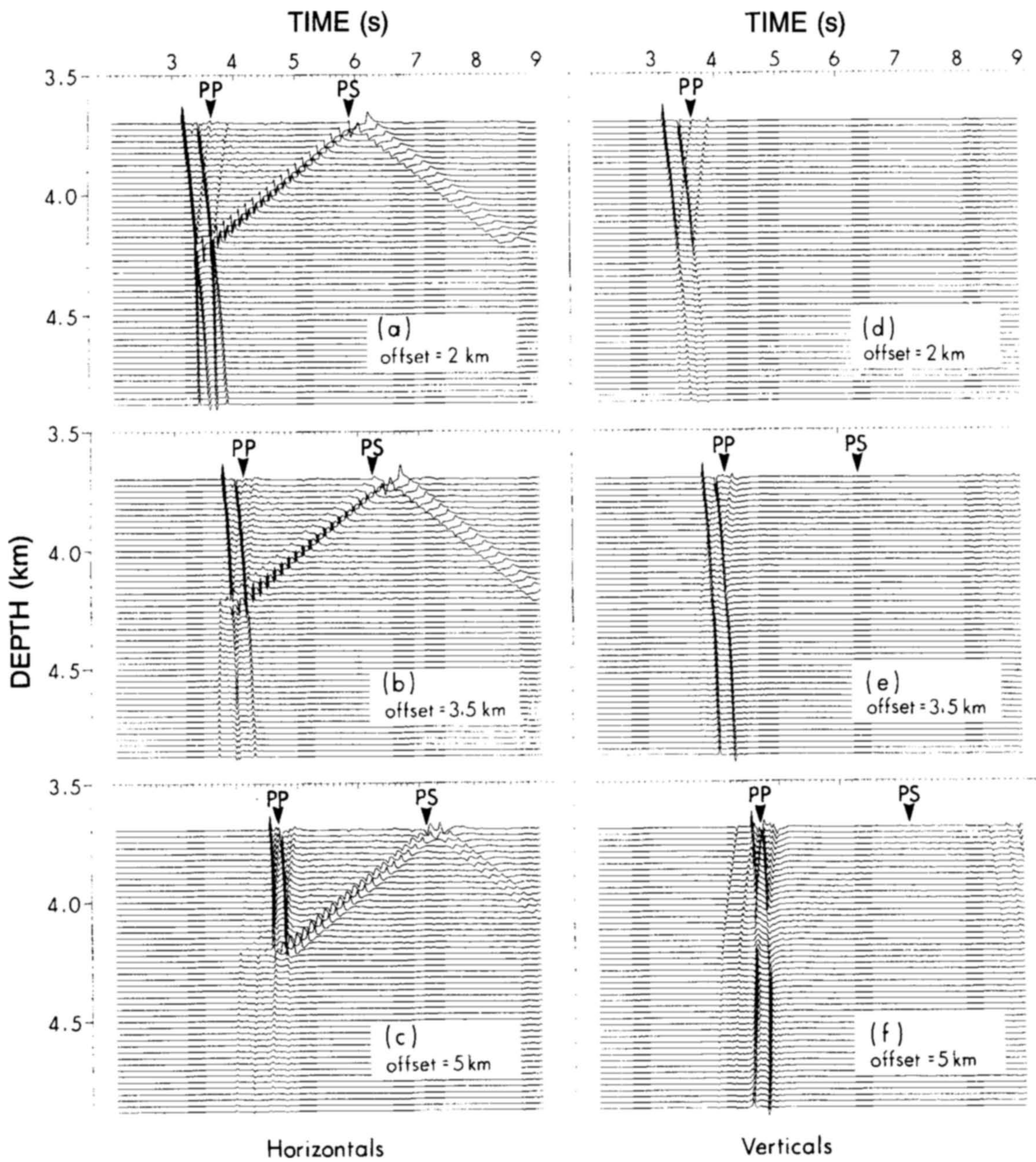

FIG. 11. (a)–(c) are synthetic VSP seismograms for horizontal displacement at 2, 3.5, and 5 km offsets, computed using the model similar to the one shown in Figure 9a but with the ice cap replaced by water. The marked events *PP* and *PS* are the sediment-basement *P*-to-*P* and *P*-to-*S* reflections, respectively. (d)–(f) are similar to (a)–(c), but with vertical displacement.

ACKNOWLEDGMENTS

The computations shown here were carried out on the National Science Foundation's San Diego Super Computer facility under grant EAR-8607460. Support of earlier, related work by the Marine Geology and Geophysics Division of the Office of Naval Research is also gratefully acknowledged. Equations (12) and (14) and their application to VSP were first developed for the Geo-Pacific Corporation of Honolulu, which we thank for granting us permission to publish this paper. Hawaii Institute of Geophysics contribution no. 1933.

REFERENCES

Aki, K., and Richards, P. G., 1980, Quantitative seismology, **1**: W. H. Freeman and Co.

Aminzadeh, F., and Mendel, J. M., 1985, Synthetic vertical seismic profiles for nonnormal incidence plane waves: Geophysics, **50**, 127–141.

Balch, A. H., and Lee, M. W., 1984, Vertical seismic profiling: techniques, applications and case histories: Internat. Human Res. Dev. Corp.

Braile, L. W., and Smith, J. B., 1975, Guide to the interpretation of crustal reflection profiles: Geophys. J. Roy. Astr. Soc., **40**, 145–176.

Burridge, R., and Knopoff, L., 1964, Body force equivalents for seismic dislocations: Bull. Seis. Soc. Am., **54**, 1875–1888.

Chin, R. C. Y., Hedstrom, G. W., and Thigpen, L., 1984, Matrix methods in synthetic seismograms: Geophys. J. Roy. Astr. Soc., **77**, 483–502.

Cormier, V. F., and Mellen, M. H., 1984, Application of asymptotic ray theory to synthetic vertical seismic profiling, *in* Töksoz, M. N., and Stewart, R. R., Eds., Vertical seismic profiling, part B, Advanced concepts: Geophysical Press, 28–44.

Dietrich, M., Prange, M., and Bouchon, M., 1984, Synthetic vertical seismic profiles using the discrete wavenumber method, *in* Töksoz, M. N., and Stewart, R. R., Eds., Vertical seismic profiling, part B, Advanced concepts: Geophysical Press, 16–27.

Dix, C. H., 1939, Interpretation of well shot data: Geophysics, **4**, 24–32.

Fryer, G. J., and Frazer, L. N., 1984, Seismic waves in stratified anisotropic media: Geophys. J. Roy. Astr. Soc., **78**, 691–710.

Fuchs, K., and Müller, G., 1971, Computation of synthetic seismograms with the reflectivity method and comparison with observations: Geophys. J. Roy. Astr. Soc., **23**, 417–433.

Gal'perin, E. I., 1974, Vertical seismic profiling: Nauka, English trans., Soc. Explor. Geophys.

Jolly, R. N., 1953, Deep hole geophone studies in Garvin County, Oklahoma: Geophysics, **19**, 662–670.

Kelly, K. R., Ward, R. W., and Whitmore, N. D., 1982, Modeling—The forward method, *in* Jain, K. C., and deFigueiredo, R. J. P., Eds., Concepts and techniques in oil and gas exploration: Soc. Explor. Geophys.

Kennett, B. L. N., 1974, Reflections, rays and reverberations: Bull. Seis. Soc. Am., **64**, 1685–1696.

——— 1975, The effect of attenuation on seismograms: Bull. Seis. Soc. Am., **65**, 1643–1651.

——— 1979, Theoretical reflection seismograms for an elastic medium: Geophys. Prosp., **27**, 301–321.

——— 1980, Seismic waves in a stratified half space II—Theoretical seismogram: Geophys. J. Roy. Astr. Soc., **61**, 1–10.

——— 1983, Seismic wave propagation in stratified media: Cambridge Univ. Press.

Kennett, B. L. N., and Clarke, T. J., 1983, Seismic waves in a stratified half space—IV: *P-SV* wave decoupling and surface wave dispersion: Geophys. J. Roy. Astr. Soc., **72**, 633–645.

Kennett, B. L. N., and Illingworth, M. R., 1981, Seismic waves in a stratified half space III—Piecewise smooth models: Geophys. J. Roy. Astr. Soc., **66**, 633–675.

Kennett, B. L. N., and Kerry, N. J., 1979, Seismic waves in a stratified half-space: Geophys. J. Roy. Astr. Soc., **57**, 557–583.

Khalyevich, N. I., 1955, Supporting devices for geophones in seismic well logging: Razved. i Promysl. Geofix., no. 14.

Kind, R., 1976, Computation of reflection coefficients for layered media: J. Geophys., **42**, 191–200.

Liu, H. P., Anderson, D. L., and Kanamori, H., 1976, Velocity dispersion due to an elasticity: implications for seismology and mantle composition: Geophys. J. Roy. Astr. Soc., **47**, 41–58.

Mallick, S., and Frazer, L. N., 1987, Practical aspects of reflectivity modeling: Geophysics, **52**, 1355–1364.

McMechan, G. A., 1985, Synthetic finite-offset vertical seismic profiles for laterally varying media: Geophysics, **50**, 627–636.

Riggs, E. D., 1955, Seismic wave types in a borehole: Geophysics, **22**, 53–67.

Schmidt, H., and Tango, G., 1986, Efficient global matrix approach to the computation of synthetic seismograms: Geophys. J. Roy. Astr. Soc., **84**, 331–359.

Stephen, R. A., 1977, Synthetic seismograms for the case of the receiver within the reflectivity zone: Geophys. J. Roy. Astr. Soc., **51**, 169–181.

——— 1984, Synthetic vertical seismic profiles by the method of finite difference, *in* Töksoz, M. N., and Stewart, R. R., Eds., Vertical seismic profiling, part B, Advanced concepts: Geophysical Press, 63–79.

Sullivan, M. F., 1984, Finite element modelling of VSP data, *in* Töksoz, M. N., and Stewart, R. R., Eds., Vertical seismic profiling, part B, Advanced concepts: Geophysical Press, 45–62.

Suprajitno, M., and Greenhalgh, S. A., 1986, Theoretical vertical seismic profiling seismograms: Geophysics, **51**, 1252–1265.

Temme, P., and Müller, G., 1982, Numerical simulation of vertical seismic profiling: J. Geophys., **50**, 177–188.

Thybo, M., 1983, Fast computation of synthetic vertical seismic profiles: Presented at the 45th Ann. Mtg., Eur. Assn. Explor. Geophys.

Ursin, B., and Arnsten, B., 1983, Computation of zero-offset vertical seismic profiles including spherical spreading and absorption: Presented at the 45th Ann. Mtg., Eur. Assn. Explor. Geophys.

Wyatt, K. D., 1981, Synthetic vertical seismic profiles: Geophysics, **46**, 880–891.